

1 **TMPRSS2 contributes to virus spread and immunopathology in the**  
2 **airways of murine models after coronavirus infection**

3

4 Naoko Iwata-Yoshikawa<sup>a†</sup>, Tadashi Okamura<sup>b,c†</sup>, Yukiko Shimizu<sup>b</sup>, Hideki Hasegawa<sup>a</sup>,  
5 Makoto Takeda<sup>d</sup>, and Noriyo Nagata<sup>a#</sup>

6

7 <sup>a</sup>Department of Pathology, National Institute of Infectious Diseases, Tokyo, Japan;

8 <sup>b</sup>Department of Laboratory Animal Medicine, Research Institute, National Center for

9 Global Health and Medicine (NCGM), Tokyo, Japan; <sup>c</sup>Section of Animal Models,

10 Department of Infectious Diseases, Research Institute National Center for Global Health

11 and Medicine, Tokyo, Japan; <sup>d</sup>Department of Virology III, National Institute of Infectious

12 Diseases, Tokyo, Japan

13

14 Running head: Role of TMPRSS2 in coronavirus infection *in vivo*

15

16 #Address correspondence to Noriyo Nagata, nnagata@niid.go.jp.

17 †N.I.-Y. and T.O. contributed equally to this work.

18

19 **Abstract**

20 Transmembrane serine protease TMPRSS2 activates the spike protein of highly  
21 pathogenic human coronaviruses such as severe acute respiratory syndrome-related  
22 coronavirus (SARS-CoV) and Middle East respiratory syndrome-related coronavirus  
23 (MERS-CoV). *In vitro*, activation induces virus-cell membrane fusion at the cell surface.  
24 However, the roles of TMPRSS2 during coronavirus infection *in vivo* are unclear. Here, we  
25 used animal models of SARS-CoV and MERS-CoV infection to investigate the role of  
26 TMPRSS2. Th-1-prone C57BL/6 mice and TMPRSS2-knockout (KO) mice were used for  
27 SARS-CoV infection, and transgenic mice expressing the human MERS-CoV receptor,  
28 hDPP4-Tg mice, and TMPRSS2-KO hDPP4-Tg mice were used for MERS-CoV infection.  
29 After experimental infection, TMPRSS2-deficient mouse strains showed reduced body  
30 weight loss and viral kinetics in the lungs. Lack of TMPRSS2 affected the primary sites of  
31 infection and virus spread within the airway, accompanied by less severe immunopathology.  
32 However, TMPRSS2-KO mice showed weakened inflammatory chemokine and/or cytokine  
33 responses to intranasal stimulation with poly (I:C), a Toll-like receptor 3 agonist. In

34 conclusion, TMPRSS2 plays a crucial role in viral spread within the airway of murine

35 models infected by SARS-CoV and MERS-CoV and in the resulting immunopathology.

36

37 **Importance**

38 Broad-spectrum antiviral drugs against highly pathogenic coronaviruses and other

39 emerging viruses are desirable to enable a rapid response to pandemic threats.

40 Transmembrane protease serine type2 (TMPRSS2), a protease belonging to the type II

41 transmembrane serine protease family, cleaves the coronavirus spike protein, making it a

42 potential therapeutic target for coronavirus infections. Here, we examined the role of

43 TMPRSS2 using animal models of SARS-CoV and MERS-CoV infection. The results

44 suggest that lack of TMPRSS2 in the airways reduces the severity of lung pathology after

45 infection by SARS-CoV and MERS-CoV. Taken together, the results will facilitate

46 development of novel targets for coronavirus therapy.

47

48 **Introduction**

49 Highly pathogenic human coronaviruses such as severe acute respiratory  
50 syndrome-related coronavirus (SARS-CoV) (1-6) and Middle East respiratory  
51 syndrome-related coronavirus (MERS-CoV) (7-9) cause severe infection of the lower  
52 respiratory tract in humans. These zoonotic pathogens have mortality rates of >50% in aged  
53 and immunosuppressed populations, making them potentially important emerging  
54 pathogens (10, 11). Broad-spectrum antiviral drugs against these coronaviruses (and other  
55 highly pathogenic viruses) will facilitate rapid responses to pandemic threats.  
56 Transmembrane protease serine type2 (TMPRSS2), a protease belonging to the type II  
57 transmembrane serine protease family, cleaves the influenza virus hemagglutinin (HA)  
58 molecule in human airway epithelial cells (12); however, it can also cleave coronavirus  
59 fusion glycoproteins, namely, the spike protein. The protease activates the spike protein to  
60 induce virus-cell membrane fusion at the cell surface and facilitate entry of coronaviruses  
61 into the host cell (13-16). Thus, active site inhibitors of TMPRSS2 are potential therapeutic  
62 targets not only for influenza viruses but also coronaviruses (17). Some animal studies

63 show that TMPRSS2-knockout (KO) mice are protected against severe pathology and death  
64 after influenza virus infection (18-21). In addition, a genetic study revealed that those with  
65 high expression of certain TMPRSS2 variants are at increased risk of severe outcomes after  
66 infection with A (H1N1) pdm09 influenza (22). However, the roles of TMPRSS2 *in vivo*  
67 during coronavirus infection are unclear. Here, we used animal models of coronavirus  
68 infection to examine the role of TMPRSS2.

69 Previously, we established a murine model of SARS based on adult BALB/c mice. The  
70 animals were moribund due to severe pulmonary edema caused by skewing the immune  
71 response toward a Th2 profile after infection by mouse-adapted SARS-CoV (23, 24). We  
72 used adult C57BL/6 mice because the TMPRSS2-KO mice were back crossed to this strain  
73 (20). After infection with mouse-adapted SARS-CoV, Th-1-prone C57BL/6 mice developed  
74 acute pneumonia, with around 15% body weight loss; however, this was not fatal. In  
75 addition, we recently generated an animal model of MERS-CoV using transgenic mice  
76 expressing hDPP4 (hDPP4-Tg mice) under the control of an endogenous promoter  
77 (Iwata-Yoshikawa et al., Submitted). The hDPP4-Tg mice were susceptible to infection by

78 MERS-CoV and developed acute pneumonia with transient loss of body weight. Next, we  
79 generated TMPRSS2-KO hDPP4-Tg (TMPRSS2-KO Tg) mice by crossing male  
80 hDPP4-Tg mice with female TMPRSS2-KO mice.

81 Here, we used these animal models to demonstrate a role for TMPRSS2 during infection  
82 by SARS-CoV and MERS-CoV. TMPRSS2-deficient mice showed reduced body weight  
83 loss and viral replication in the lungs. In addition, histopathological and  
84 immunohistochemical analyses revealed that expression of TMPRSS2 influenced both the  
85 primary site of infection and virus spread within the airways of both mouse models, which  
86 was accompanied by different immunopathologies.

87

## 88 **Results**

### 89 **TMPRSS2-KO mice show no body weight loss and weak proinflammatory responses** 90 **after SARS-CoV infection**

91 To screen the generated TMPRSS2-KO mice, we confirmed the absence of the  
92 TMPRSS2 gene by PCR analysis using a primer set specific for TMPRSS2 (Fig. 1). To

93 examine the effect of TMPRSS2 expression during SARS-CoV infection, we infected  
94 C57BL/6 wild-type (WT) and TMPRSS2-KO mice with  $10^5$  TCID<sub>50</sub> F-musX  
95 mouse-adapted SARS-CoV. WT mice showed clear loss of body weight from 2 to 4 days  
96 post-injection (p.i.), but recovered later (the exception was a single moribund mouse at Day  
97 5 p.i.); these symptoms were not observed in TMPRSS2-KO mice (Fig. 2a). Measurement  
98 of the virus titer showed lower viral replication in the lungs of TMPRSS2-KO mice (Fig.  
99 2b). There were no significant differences in the titers of neutralizing antibodies in serum  
100 samples from either group (Fig. 2c).

101 Histopathological and immunohistochemical analyses revealed that lack of TMPRSS2  
102 affected the primary infection sites in the airway. Immunohistochemical staining on Day 1  
103 p.i. revealed strongly antigen-positive cells in the bronchiolar epithelium of WT mice  
104 infected with SARS-CoV; however, only very weak antigen positivity was observed in  
105 TMPRSS2-KO mice (Fig. 2d, left panels). Some antigen-positive cells were seen in alveoli  
106 from both WT and TMPRSS2-KO mice on Day 3 p.i. (Fig. 2d, middle panels). On Day 3  
107 p.i., cell debris and diffuse inflammatory infiltration by neutrophils and mononuclear cells

108 were observed around bronchi and in the alveoli of WT mice; by contrast, focal  
109 inflammatory infiltration was observed in the alveoli of TMPRSS2-KO mice (Fig. 2d, right  
110 panels). On Day 10 p.i., formation of granulation tissue was observed in the healing  
111 alveolar area of most WT mice (eight of nine mice) (Fig. 3, upper panel), whereas it was  
112 observed in only a few TMPRSS2-KO mice (three of fourteen mice) (Fig. 3, lower panel).

113 Next, we measured the concentrations of representative inflammatory growth factors,  
114 chemokines, and cytokines in the lungs and observed transient elevation of FGF-basic,  
115 MIP-1 $\alpha$ /CCL3, MIG/CXCL9, MCP-1/CCL2, IP-10/CXCK10, IL-1 $\alpha$ , IL-1 $\beta$ , IL-12, IL-6,  
116 IL-4, and IL-10 in the lungs of WT mice at 3 days p.i. (Fig. 4a, black bars). Similar  
117 responses were observed in the lungs of TMPRSS2-KO mice; however, the concentrations  
118 of FGF-basic, KC/CXCL1, IL-12 (p40/p70), IL-4, and IL-10 were significantly lower than  
119 those in WT mice at Day 2 or 3 p.i. (Fig. 4a, white bars).

120 Furthermore, we measured the expression of mRNA encoding the Toll-like receptor 3  
121 (TLR3), which recognizes ds RNA and activates the NF- $\kappa$ B pathway for the activation of  
122 type 1 interferon (IFN), and type 1 IFN including IFN- $\alpha$ 4 and IFN- $\beta$  in the lungs of mice at

123 6 h and at 1, 2 and 3 days p.i. by real-time reverse transcription RT-PCR (24, 25).

124 Interestingly, we found a transient increase in TLR3 expression in the lungs of

125 TMPRSS2-KO mice at 6 h p.i., but not in WT mice (Fig. 4b). However, IFN- $\alpha$ 4 and IFN- $\beta$

126 mRNA expression was higher in WT mice than in TMPRSS2-KO mice (Fig. 4b).

127 Taken together, these results suggest that lack of TMPRSS2 affects both pathology and

128 immunopathology in the bronchi and/or alveoli after infection by SARS-CoV. Lower viral

129 replication in the lungs and less severe immunopathology observed in TMPRSS2-KO mice

130 resulted in no body weight loss and milder lung pathology.

131

132 **TMPRSS2-KO hDPP4-Tg mice show weaker proinflammatory responses and less**

133 **severe lung pathology after infection with MERS-CoV**

134 TMPRSS2-KO hDPP4-Tg mice were generated as described in Materials and Methods.

135 To screen the generated Tg mice and TMPRSS2-KO hDPP4-Tg mice, we confirmed the

136 presence of the transgene of hDPP4 and absence of the TMPRSS2 gene by PCR analysis

137 using two primers sets specific for hDPP4 and TMPRSS2 (Fig. 1). The mice were then used

138 to examine the role of TMPRSS2 after MERS-CoV infection. After intranasal inoculation  
139 with HCoV-EMC 2012 (MERS-CoV), hDPP4-Tg mice showed a temporary and mild loss  
140 of body weight (from 6 to 9 days p.i.); however, only very slight changes were observed in  
141 TMPRSS2-KO Tg mice (Fig. 5a). The results of virus titer measurements suggested that the  
142 virus replicated more slowly in the lungs of TMPRSS2-KO Tg mice (Fig. 5b). The lung  
143 from one out of five Tg mice contained  $10^{6.45}$ TCID<sub>50</sub>/g at Day 7 p.i. (two females and three  
144 males), and that from three out of five TMPRSS2-KO mice contained  $10^{4.2}$  or  $10^{4.7}$   
145 TCID<sub>50</sub>/g at Day 7 p.i. (one female and four males). In addition, the titers of neutralizing  
146 antibodies in serum from TMPRSS2-KO Tg mice were significantly lower than those in  
147 serum from hDPP4-Tg mice (Fig. 5c).

148 More obvious histopathological differences were observed in MERS-CoV-infected  
149 animals than in SARS-CoV-infected animals (Fig. 5d). On Day 1 p.i., many viral  
150 antigen-positive cells were observed in the bronchi and alveolar areas of hDPP4-Tg mice;  
151 there were none in the bronchi, and only a few in the alveoli, of TMPRSS2-KO Tg mice  
152 (Fig. 5d, left panels). On Day 3 p.i., many viral antigen-positive cells were present in these

153 areas in hDPP4-Tg mice, but fewer in TMPRSS2-KO Tg mice (Fig. 5d, middle panels). On  
154 Day 7 p.i., thickening of the alveolar wall, with regenerated alveolar cells and prominent  
155 cellular infiltration by macrophages and mononuclear cells, was observed in Tg mice, but  
156 only mild infiltration (mainly by mononuclear cells) of the alveoli was observed in  
157 TMPRSS2-KO Tg mice (Fig. 5d, right panels). On Day 14 p.i., lymphocyte aggregates and  
158 cellular infiltrations were seen in the healing alveolar area of hDPP4-Tg mice (Fig. 6, upper  
159 panel), whereas they were nearly absent from the healing alveolar area of TMPRSS2-KO  
160 Tg mice (Fig. 6, lower panel). However, no granulation tissues were detected in either  
161 mouse.

162 These data suggest that lack of TMPRSS2 has a marked effect on MERS-CoV infection  
163 and replication in the bronchi and/or alveoli. Reduced viral replication in the lungs of  
164 TMPRSS2-KO Tg mice resulted in only slight body weight loss and less severe lung  
165 pathology.

166 Measurement of representative proinflammatory growth factors, chemokines, and  
167 cytokines in hDPP4-Tg mice (i.e., GM-CSF, FGF-basic, MIP-1 $\alpha$ /CCL3, MIG/CXCL9,

168 MCP-1/CCL2, IL-1 $\alpha$ , IL-1 $\beta$ , TNF- $\alpha$ , IL-12, IFN- $\gamma$ , IL-17, and IL-13) revealed transient  
169 elevation during the first 7 days p.i. (Fig. 7, black bars). Tmprss2-KO Tg mice showed  
170 similar responses, but they occurred later or were less pronounced than in hDPP4-Tg mice  
171 (Fig. 7, white bars). The concentration of FGF-basic, GM-CSF, MIG/CXCL9, and TNF- $\alpha$   
172 in the lungs of Tmprss2-KO Tg mice was lower than that in the lungs of hDPP4-Tg mice  
173 on Days 5 and 7 p.i. Interestingly, expression of IL-6 and other inflammatory chemokines  
174 (i.e., MIP-1 $\alpha$ , IL-1 $\alpha$ , and IL-1 $\beta$ ) was higher in Tmprss2-KO Tg mice than in hDPP4-Tg  
175 mice on Day 7 p.i.

176 Furthermore, we measured the expression of mRNA encoding TLR3 and type 1 IFN,  
177 including IFN- $\alpha$ 4 and IFN- $\beta$ , in the lungs of mice at 6 h and at 1, 2 and 3 days p.i. by  
178 real-time reverse transcription RT-PCR (24, 25). No obvious increase in TLR3 expression  
179 in the lungs of mice was observed (Fig. 7b); however, IFN- $\alpha$ 4 and IFN- $\beta$  mRNA  
180 expression was higher in hDPP4-Tg mice than in Tmprss2-KO Tg mice on days 2 and/or  
181 3 p.i. (Fig. 7b).

182

183 **Innate immune responses in TMPRSS2-KO mice induced by a Toll-like receptor 3**

184 **(TLR3) agonist**

185 Assay of chemokine and cytokine concentrations after coronavirus infection revealed  
186 that proinflammatory immune responses in TMPRSS2-deficient mice were weaker than  
187 those in WT mice. To assess the effect of knocking out TMPRSS2 on innate immune  
188 responses in the absence of virus infection, we inoculated mice intranasally with poly (I:C),  
189 a synthetic analog of double-strand RNA (26-28). Cytokine levels in the lungs were  
190 measured at 24 h p.i. The concentrations of MCP-1/CCL2, KC/CXCL1, IL-1 $\alpha$ , IL-5, IFN- $\gamma$ ,  
191 and IL-17 in TMPRSS2-KO mice were lower than those in WT mice (Fig. 8). In addition,  
192 levels of FGF-basic and IL-6 in the TMPRSS2-KO Tg mice were lower than those in  
193 hDPP4-Tg mice (Fig. 8). These results suggest that TMPRSS2-deficient mice intrinsically  
194 exhibit weaker or delayed inflammatory chemokine and cytokine responses via TLR3.

195

196 **Discussion**

197 Mouse models of SARS-CoV and MERS-CoV infection allow us to investigate disease

198 pathogenesis and vaccine applications, and to evaluate antiviral drugs and other therapies.  
199 hDPP4-Tg mice are susceptible to infection by a MERS-CoV isolate, resulting in acute  
200 pneumonia but no brain disease (Iwata-Yoshikawa N, submitted). Here, we generated a  
201 TMPRSS2-KO mouse bearing hDPP4. After infection with SARS-CoV or MERS-CoV,  
202 TMPRSS2-deficient mice were protected from body weight loss. The results suggest that  
203 TMPRSS2 plays an important role in the early phase of disease (lung infection); in  
204 particular, SARS-CoV and MERS-CoV replicated in the bronchioles.

205 In humans, TMPRSS2 is expressed widely in epithelial tissues, including that lining the  
206 upper airways, bronchi, and lung (29). The protein sequence of human and mouse  
207 TMPRSS2 is conserved, with 78% sequence identity between the two species. *In situ*  
208 hybridization analyses of mouse embryos and adult tissues reveal that TMPRSS2 is  
209 expressed in the epithelium lining the gastrointestinal, urogenital, and respiratory tracts,  
210 including the bronchi and bronchioles, but not in alveolar epithelium (30). Kim et al.  
211 showed that depletion of TMPRSS2 (the molecule was inactivated by disrupting the serine  
212 protease domain through homologous recombination) from mice did not affect

213 development or survival to adulthood; neither were there abnormalities in organ histology  
214 or function (31). While the physiological function of TMPRSS2 is unclear, data suggest  
215 that it does regulate sodium currents in lung epithelial cells through proteolytic cleavage of  
216 the epithelial sodium channel (32). We also made the interesting observation that  
217 TMPRSS2-deficient mice show weaker, or delayed, inflammatory chemokine and cytokine  
218 responses mediated by Toll-like receptor 3.

219 Host cellular proteases such as trypsin, tryptase Clara, miniplasmin, human airway  
220 trypsin-like protease, and TMPRSS2 cleave the HA glycoprotein of influenza A viruses.  
221 Cleavage of HA is critical for viral entry into cells during fusion between the viral and host  
222 cell membranes (33). Serine protease inhibitors such as camostat and aprotinin inhibit both  
223 influenza virus replication in human airway epithelial cells and the release of cytokines  
224 (IL-6 and TNF- $\alpha$ ) into cell supernatants (34). In addition, animal studies using  
225 TMPRSS2-KO mice reveal that TMPRSS2 is essential for the spread and pathogenesis of  
226 influenza viruses such as emerging H7N9 and seasonal H1N1 and H3N2 (18-21).  
227 TMPRSS2 also cleaves the coronavirus spike protein to generate unlocked,

228 fusion-catalyzing forms at the cell surface and facilitate rapid “early” entry (14, 15, 35-39).  
229 In addition, SARS-CoV and MERS-CoV enter cells via two distinct pathways: TMPRSS2  
230 via the cell surface and cathepsin L via the endosome (13, 14, 16, 36, 40, 41). A previous  
231 antiviral study revealed that a serine protease (TMPRSS2) rather than a cysteine protease  
232 (Cathepsin L) facilitated the spread of SARS-CoV in the infected mouse (42). Our findings  
233 are in agreement with this study; coronavirus replication in the lungs, especially in the  
234 bronchioles, was less pronounced in TMPRSS2-deficient mice. However, viral spread and  
235 inflammatory infiltration were still detected in the alveoli. Several proteases, including  
236 other serine proteases and the cysteine protease, cathepsin L, may activate both SARS-CoV  
237 and MERS-CoV, allowing the virus to spread to alveolar areas in TMPRSS2-deficient mice.  
238 In addition, TLR3 mRNA expression in the lungs at 6 h p.i. of SARS-CoV-inoculated  
239 TMPRSS2-deficient mice suggested that TLR3, which recognizes specifically dsRNA and  
240 localizes to endosomes (43), recognized viral RNA within the endosomal component. Thus,  
241 we speculate that the pathway employing cathepsin L and the endosome mainly contributed  
242 to SARS-CoV infection in the TMPRSS2-deficient mice.

243 MERS-CoV infected animals had more obvious histopathological differences than  
244 SARS-CoV infected animals in this animal model. In addition, weak-positive SARS-CoV  
245 antigens at 1 day p.i. and a few virus antigen positive cells at 3 days p.i. were detected in  
246 the bronchi of TMPRSS2-KO mice, but not in MERS-CoV-inoculated TMPRSS2-KO Tg  
247 mice. Thus, MERS-CoV may rely more on TMPRSS2 during early infection than  
248 mouse-adapted SARS-CoV, although differences in viral passage history and in the genetic  
249 backgrounds of the animals should also be considered. More work will be required to test  
250 the possibility that viral mutations are acquired during virus spreading in TMPRSS2  
251 deficient mice.

252 TMPRSS2-deficient mice, including TMPRSS2-KO and TMPRSS2-KO Tg mice,  
253 showed less severe loss of body weight after infection. Peak expression of FGF-basic, also  
254 known as FGF2, after infection synchronized with peak body weight loss in WT and  
255 hDPP4-Tg mice. FGFs play a role in tissue repair after pneumonia, including bronchiolitis  
256 obliterans organizing pneumonia (BOOP) and interstitial pneumonia (both fibrous  
257 pulmonary disorders), by promoting proliferation of fibroblasts (44). In fact, formation of

258 granulation tissue was observed in WT mice after SARS-CoV infection. BOOP and  
259 pulmonary fibrosis are common in those with SARS, including patients who survive the  
260 infection (45). While there is limited evidence for development of fibrosis during end-stage  
261 acute respiratory distress syndrome induced by MERS-CoV, clinical data from MERS  
262 patients suggest that the situation is similar to that observed for SARS (45, 46). In addition,  
263 some metabolic FGFs cause body weight loss (47).

264 As expected, lower expression of cytokines and chemokines was observed in  
265 TMPRSS2-deficient mice than in TMPRSS2-competent mice after coronavirus infection.  
266 This result is similar to those reported for TMPRSS2 and TMPRSS4 double-KO mice on  
267 Day 3 post-H3N2 influenza A virus infection (48). High levels of virus replication very  
268 likely induce severe tissue damage and increased cellular infiltration by immune cells. Viral  
269 replication is likely a major cause of the elevated inflammatory chemokine levels observed  
270 in WT mice; nevertheless, we assessed the possibility that TMPRSS2, a serine protease,  
271 may also contribute to inflammatory reactions after TLR3 stimulation. Intranasal  
272 administration of poly (I:C) induced expression of MCP-1, KC, IL-1 $\alpha$ , IL-1 $\beta$ , and IL-12 in

273 the lungs of WT mice, but not in those of TMPRSS2-KO mice. The genetic backgrounds of  
274 WT and TMPRSS2-KO mice were the same because the TMPRSS2-KO mice were  
275 produced from TMPRSS2 gene knockout C57BL/6 ES cells. The physiological function of  
276 TMPRSS2 remains unclear; however, TMPRSS2 may contribute to more severe or rapid  
277 immunopathology in WT mice by increasing the levels of inflammatory cytokines and  
278 chemokines after TLR3 stimulation.

279 The immune responses to poly I:C treatment in 14-16 weeks-old hDPP4-Tg mice were  
280 quite different from those in 14-16 weeks-old WT C57BL/6 mice. The hDPP4-Tg mice  
281 were produced from BDF1×C57BL/6 mice; however, the Tg mice were backcrossed with  
282 C57BL/6 mice for eight generations. Thus, the genetic backgrounds were almost the same  
283 between these strains. On the other hand, hDPP4 expression did not have a marked effect  
284 on basal innate immune responses in 10-week-old C57BL/6 and hDPP4-Tg mice; however,  
285 hDPP4-Tg show slightly stronger or earlier innate immune responses than C57BL/6 mice  
286 (Iwata-Yoshikawa et al., Submitted). In addition, Simeoni et al reported that hDPP4/CD26  
287 transgene expression induced major phenotypic changes in T-cell populations within the

288 thymus and peripheral blood of their Tg mice, and that peripheral blood T-cell reduction  
289 was age-dependent (49). Thus, the compromised immune responses in our hDPP4-Tg mice  
290 were possibly due to hDPP4.

291 Broad-spectrum antiviral drugs against coronaviruses and other highly pathogenic  
292 viruses will enable a rapid response to pandemic threats. Here, we demonstrate a role of  
293 TMPRSS2 during infection by SARS-CoV and MERS-CoV. TMPRSS2 played an active  
294 role at primary infection sites and influenced the spread of coronaviruses within the airways  
295 of both mouse models, modulating the eventual immunopathology. Interestingly,  
296 inflammatory chemokine and cytokine levels in TMPRSS2-KO mice were lower even after  
297 intranasal stimulation by poly (I:C), suggesting an as-yet-unidentified physiological role for  
298 TMPRSS2. In conclusion, we show that TMPRSS2 plays a role in the spread and  
299 immunopathology of coronaviruses in the airways.

300

301 **Materials and methods**

302 **Ethics statements**

303 Experiments using recombinant DNA and pathogens were approved by the Committee  
304 for Experiments using Recombinant DNA and Pathogens at the National Institute of  
305 Infectious Diseases, Tokyo, Japan. All animal experiments were approved by the Animal  
306 Care and Use Committee of the National Institute of Infectious Diseases and were  
307 conducted in accordance with institutional Guidelines for the Care and Use of Animals. All  
308 animals were housed in a Japan Health Sciences Foundation-certified facility.

309

### 310 **Cells and viruses**

311 Vero E6 cells (American Type Cell Collection, Manassas, VA) were cultured in Eagle's  
312 MEM containing 5% fetal bovine serum (FBS), 50 IU/ml penicillin G, and 50 µg/ml  
313 streptomycin (5% FBS-MEM). Stocks of a mouse-passaged Frankfurt 1 isolate of  
314 SARS-CoV and F-musX-VeroE6 were propagated twice and titrated on Vero E6 cells prior  
315 to cryopreservation at 80°C, as previously described (23). MERS-CoV (HCoV-EMC 2012  
316 strain) was kindly provided by Dr. Bart Haagmans and Dr. Ron Fochier (Erasmus Medical  
317 Center, Rotterdam, The Netherlands). Stocks of MERS-CoV were propagated twice,

318 titrated on Vero E6 cells, and cryopreserved at -80°C. Viral infectivity titers are expressed  
319 as the TCID<sub>50</sub>/ml on Vero E6 cells and were calculated according to the Behrens-Kärber  
320 method. All work with infectious SARS-CoV and MERS-CoV was performed under  
321 biosafety level 3 conditions.

322

### 323 **Generation of mice.**

324     TMPRSS2<sup>-/-</sup> mice were established from TMPRSS2 gene knockout C57BL/6  
325 embryonic stem (ES) cells (product number VG13341), which were obtained from the  
326 Knockout Mouse Project (KOMP) Repository (UC Davis). The ES cells were injected into  
327 C57BL/6 mouse blastocysts, and chimeric mice with a complete C57BL/6 genetic  
328 background were generated. TMPRSS2<sup>-/-</sup> mice with a homologous genotype were obtained  
329 by crossing male and female TMPRSS2<sup>+/-</sup> C57BL/6 mice (20).

330     The transgenic mice expressing human DPP4 gene (hDPP4-Tg mice) were generated by  
331 microinjection of the purified BAC clones carrying hDPP4 gene into the pronuclei of  
332 fertilized eggs from BDF1×C57BL/6NCr mice (Iwata-Yoshikawa et al., submitted). The

333 transgenic mice were then backcrossed with C57BL/6NCr mice for eight generations, and  
334 subsequently crossed with homozygous TMPRSS2 knockout (TMPRSS2<sup>-/-</sup>) mice.

335 Genomic DNA isolated from ear punch tissues was subjected to genotyping by PCR  
336 analysis using hDPP4-specific primers (Forward; 5'-ACACACACACTCTCACACACT-3',  
337 Reverse; 5'-TCTCAGTGCCATAAAAGCCCA-3') (Iwata-Yoshikawa N et al., submitted)  
338 or TMPRSS2-specific primers P11 (5'-ACCTGGAGTATACGGGAACGTGA-3') and P12  
339 (5'-GTGAGTGGGTGAAGGTTGGGTAG-3') (31).

340

#### 341 **Animal experiments**

342 Mice were anesthetized by intraperitoneal injection of a mixture of 1.0 mg of ketamine  
343 and 0.02 mg of xylazine (0.08 ml/10 g of body weight). TMPRSS2-KO mice, C57BL/6  
344 mice lacking a homologous genotype of the TMPRSS2 gene (TMPRSS2<sup>-/-</sup>) (20), and  
345 C57BL/6 mice (WT mice; TMPRSS2<sup>+/+</sup>) were inoculated intranasally with SARS-CoV (10<sup>5</sup>  
346 TCID<sub>50</sub> in 30 µl of F-musX). Human DPP4-expressing transgenic mice (hDPP4-Tg mice:  
347 C57BL/6 mice heterozygous for the human DPP4 gene [hDPP4<sup>+/+</sup> TMPRSS2<sup>+/+</sup>])

348 (Iwata-Yoshikawa et al., manuscript in preparation) and hDPP4<sup>+/-</sup> TMPRSS2<sup>-/-</sup> C57BL/6  
349 mice (TMPRSS2-KO Tg mice) were obtained by crossing hDPP4-Tg mice with  
350 TMPRSS2-KO mice. These mice were inoculated intranasally with MERS-CoV (10<sup>6</sup>  
351 TCID<sub>50</sub> in 30 µl of HCoV-EMC 2012). Infected mice were observed for clinical signs of  
352 infection, and body weight was measured daily, for 10 days or 14 days (n = 6–14 mice, all  
353 aged 12 to 28 weeks). For analysis of virus replication, cytokine expression, and pathology,  
354 animals were sacrificed at various time points after inoculation (n = 3–4 mice per group, all  
355 aged 13 to 30 weeks).

356 WT, TMPRSS2-KO, hDPP4-Tg, and TMPRSS2-KO Tg mice (n = 4 mice per group, all  
357 aged 14 to 16 weeks) were anesthetized by intraperitoneal injection of a mixture of 1.0 mg  
358 of ketamine and 0.02 mg of xylazine (0.08 ml/10 g of body weight). Mice then received 20  
359 µg of poly (I:C) (Invitrogen, San Diego, CA) in 20 µl of PBS (intranasally) (25). All mice  
360 were sacrificed 24 h after administration for analysis of cytokine expression.

361

362 **Virus titration**

363 Lung tissue homogenates (10% [wt/vol]) were prepared in MEM containing 2% FBS, 50  
364 IU/ml penicillin G, 50 µg/ml streptomycin, and 2.5 µg/ml amphotericin B. Samples were  
365 clarified by centrifugation at  $740 \times g$  for 20 min, and the supernatant was inoculated onto  
366 Vero E6 cell cultures for virus titration.

367

#### 368 **Neutralizing antibody test**

369 Serum was collected from mice sacrificed on Day 10 or 14 p.i. After inactivation at 56°C  
370 for 30 min, Vero E6 cells were infected with virus (100 TCID<sub>50</sub> per well) in the presence of  
371 plasma (serially diluted 2-fold), incubated for 3 or 5 days, and then examined for cytopathic  
372 effects. Plasma titers of neutralizing antibodies were calculated as the reciprocal of the  
373 highest dilution at which no cytopathic effect was observed. The lowest and highest  
374 dilutions tested were 4 and 256 or 64, respectively.

375

#### 376 **Histopathology and immunohistochemistry**

377 Mice were anesthetized and perfused with 2 ml of 10% phosphate-buffered formalin.

378 The lungs were harvested, fixed, embedded in paraffin, sectioned, and stained with  
379 hematoxylin and eosin. Masson's trichrome staining was also conducted to detect fibrosis  
380 in the lungs. Immunohistochemical analysis was performed using a polymer-based  
381 detection system (Nichirei-Histofine Simple Stain Mouse MAX PO(R); Nichirei  
382 Biosciences, Inc., Tokyo, Japan). Antigen retrieval from formalin-fixed mouse tissue  
383 sections was performed by autoclaving in retrieval solution (pH 6.0; Nichirei Biosciences)  
384 at 121°C for 10 min. Hyper-immune rabbit serum raised against SARS-CoV (23) or an  
385 anti-MERS-CoV nucleocapsid antibody (Sino Biological Inc., Beijing, China) was used as  
386 the primary antibody to detect viral antigens. Peroxidase activity was detected with  
387 3,3'-diaminobenzidine (Sigma-Aldrich). Hematoxylin was used for counterstaining.

388

### 389 **Detection of inflammatory cytokines and chemokines**

390 Cytokines and chemokines in mouse lung homogenates (10% wt/vol) were measured  
391 using a commercial Mouse Cytokine 20-Plex antibody bead kit (Thermo Fisher Scientific)  
392 and a Luminex 100™ apparatus (Luminex Co, Austin, TX), as described previously (23). A

393 panel of inflammatory cytokines and chemokines (bFGF, GM-CSF, IFN- $\gamma$ , IL-1 $\alpha$ , IL-1 $\beta$ ,

394 IL-2, IL-4, IL-5, IL-6, IL-10, IL-12 [p40/p70], IL-13, IL-17, IP-10, KC, MCP-1, MIG,

395 MIP-1 $\alpha$ , TNF- $\alpha$ , and VEGF) was detected according to the manufacturer's protocols.

396

397 **Quantitative real-time RT-PCR.** To measure the levels of type I IFN and TLR3

398 mRNA expression, RNA was extracted from 20% (w/v) lung of mice infected with viruses

399 using RNeasy Mini kits (Qiagen, Hilden, Germany), according to the manufacturer's

400 instructions. mRNAs encoding IFN- $\alpha$ , IFN- $\beta$ , and TLR3 were examined by real-time

401 RT-PCR using an ABI Prism 7900HT Fast real-time PCR system (Applied Biosystems,

402 Foster City, CA). The TaqMan probes and primers, and the reaction conditions, have been

403 described previously (24, 25). Expression of each gene was normalized to that of  $\beta$ -actin.

404

405 **Statistical analysis**

406 Data are expressed as the mean and standard error of the mean. Statistical analyses were

407 performed using Graph Pad Prism 7 software (GraphPad Software Inc., La Jolla, CA).

408 Body weight curves, virus titers, and multiplex assay results were analyzed using one-way  
409 or two-way analysis of variance (ANOVA). Significant effects of viral titers in different  
410 animal strains at different time points were assessed by two-way ANOVA, and p-values  
411 were calculated using Bonferroni's multiple comparisons test. The results of the  
412 neutralizing antibody titer assays were analyzed using the Mann-Whitney test. A p-value <  
413 0.05 was considered statistically significant.

414

#### 415 **Acknowledgments**

416 We thank Dr. Ron A. M. Fouchier and Dr. Bart L. Haagmans (Erasmus Medical Center,  
417 The Netherlands) for providing MERS-CoV (isolate HCoV-EMC/2012), and Drs. Kazuya  
418 Shirato, Shutoku Matsuyama, Masaki Anraku, and Kohji Sakai (National Institute of  
419 Infectious Diseases) for helpful discussion. We also thank our colleagues at the Institute,  
420 especially Ms. Midori Ozaki and Dr. Hitoshi Kujirai, for technical assistance.

421

422 This work was supported by a Grant-in-Aid for research (H25-Shinko-Wakate-004)  
423 from the Ministry of Health, Labor, and Welfare, Japan; by a Research Program on  
424 Emerging and Re-emerging Infectious Diseases (JP17fk0108313, JP18fk0108058) from the  
425 Japan Agency for Medical Research and Development (AMED); by a Grant-in-Aid for  
426 scientific research from the Ministry of Education, Culture, Sports, Science, and  
427 Technology in Japan (KAKENHI; 16K09951, 18H02665); and in part by The Grant for  
428 National Center for Global Health and Medicine (27A1102).

429

430

431 **References**

432

- 433 1. **Ksiazek TG, Erdman D, Goldsmith CS, Zaki SR, Peret T, Emery S, Tong S,**  
434 **Urbani C, Comer JA, Lim W, Rollin PE, Dowell SE, Ling AE, Humphrey CD,**  
435 **Shieh WJ, Guarner J, Paddock CD, Rota P, Fields B, DeRisi J, Yang JY, Cox N,**  
436 **Hughes JM, LeDuc JW, Bellini WJ, Anderson LJ, Group SW.** 2003. A novel  
437 coronavirus associated with severe acute respiratory syndrome. *N Engl J Med*  
438 **348**:1953-1966.
- 439 2. **Drosten C, Gunther S, Preiser W, van der Werf S, Brodt HR, Becker S,**  
440 **Rabenau H, Panning M, Kolesnikova L, Fouchier RA, Berger A, Burguiere**  
441 **AM, Cinatl J, Eickmann M, Escriou N, Grywna K, Kramme S, Manuguerra**  
442 **JC, Muller S, Rickerts V, Sturmer M, Vieth S, Klenk HD, Osterhaus AD,**  
443 **Schmitz H, Doerr HW.** 2003. Identification of a novel coronavirus in patients with  
444 severe acute respiratory syndrome. *N Engl J Med* **348**:1967-1976.
- 445 3. **Lee N, Hui D, Wu A, Chan P, Cameron P, Joynt GM, Ahuja A, Yung MY,**  
446 **Leung CB, To KF, Lui SF, Szeto CC, Chung S, Sung JJ.** 2003. A major outbreak  
447 of severe acute respiratory syndrome in Hong Kong. *N Engl J Med* **348**:1986-1994.
- 448 4. **Peiris JS, Lai ST, Poon LL, Guan Y, Yam LY, Lim W, Nicholls J, Yee WK, Yan**  
449 **WW, Cheung MT, Cheng VC, Chan KH, Tsang DN, Yung RW, Ng TK, Yuen**  
450 **KY, group Ss.** 2003. Coronavirus as a possible cause of severe acute respiratory  
451 syndrome. *Lancet* **361**:1319-1325.
- 452 5. **Zhong NS, Zheng BJ, Li YM, Poon, Xie ZH, Chan KH, Li PH, Tan SY, Chang**  
453 **Q, Xie JP, Liu XQ, Xu J, Li DX, Yuen KY, Peiris, Guan Y.** 2003. Epidemiology  
454 and cause of severe acute respiratory syndrome (SARS) in Guangdong, People's  
455 Republic of China, in February, 2003. *Lancet* **362**:1353-1358.
- 456 6. **Guan Y, Peiris JS, Zheng B, Poon LL, Chan KH, Zeng FY, Chan CW, Chan**  
457 **MN, Chen JD, Chow KY, Hon CC, Hui KH, Li J, Li VY, Wang Y, Leung SW,**  
458 **Yuen KY, Leung FC.** 2004. Molecular epidemiology of the novel coronavirus that

- 459 causes severe acute respiratory syndrome. *Lancet* **363**:99-104.
- 460 7. **Zaki AM, van Boheemen S, Bestebroer TM, Osterhaus AD, Fouchier RA.** 2012.  
461 Isolation of a novel coronavirus from a man with pneumonia in Saudi Arabia. *N*  
462 *Engl J Med* **367**:1814-1820.
- 463 8. **Hijawi B, Abdallat M, Sayaydeh A, Alqasrawi S, Haddadin A, Jaarour N,**  
464 **Alsheikh S, Alsanouri T.** 2013. Novel coronavirus infections in Jordan, April 2012:  
465 epidemiological findings from a retrospective investigation. *East Mediterr Health J*  
466 **19 Suppl 1**:S12-18.
- 467 9. **Korea Centers for Disease C, Prevention.** 2015. Middle East Respiratory  
468 Syndrome Coronavirus Outbreak in the Republic of Korea, 2015. *Osong Public*  
469 *Health Res Perspect* **6**:269-278.
- 470 10. **Perlman S, Netland J.** 2009. Coronaviruses post-SARS: update on replication and  
471 pathogenesis. *Nat Rev Microbiol* **7**:439-450.
- 472 11. **de Wit E, van Doremalen N, Falzarano D, Munster VJ.** 2016. SARS and MERS:  
473 recent insights into emerging coronaviruses. *Nat Rev Microbiol* **14**:523-534.
- 474 12. **Bottcher E, Matrosovich T, Beyerle M, Klenk HD, Garten W, Matrosovich M.**  
475 2006. Proteolytic activation of influenza viruses by serine proteases TMPRSS2 and  
476 HAT from human airway epithelium. *J Virol* **80**:9896-9898.
- 477 13. **Matsuyama S, Nagata N, Shirato K, Kawase M, Takeda M, Taguchi F.** 2010.  
478 Efficient activation of the severe acute respiratory syndrome coronavirus spike  
479 protein by the transmembrane protease TMPRSS2. *J Virol* **84**:12658-12664.
- 480 14. **Shirato K, Kawase M, Matsuyama S.** 2013. Middle East respiratory syndrome  
481 coronavirus infection mediated by the transmembrane serine protease TMPRSS2. *J*  
482 *Virol* **87**:12552-12561.
- 483 15. **Bertram S, Dijkman R, Habjan M, Heurich A, Gierer S, Glowacka I, Welsch K,**  
484 **Winkler M, Schneider H, Hofmann-Winkler H, Thiel V, Pohlmann S.** 2013.  
485 TMPRSS2 activates the human coronavirus 229E for cathepsin-independent host  
486 cell entry and is expressed in viral target cells in the respiratory epithelium. *J Virol*  
487 **87**:6150-6160.
- 488 16. **Gierer S, Bertram S, Kaup F, Wrensch F, Heurich A, Kramer-Kuhl A, Welsch**

- 489 **K, Winkler M, Meyer B, Drosten C, Dittmer U, von Hahn T, Simmons G,**  
490 **Hofmann H, Pohlmann S.** 2013. The spike protein of the emerging  
491 betacoronavirus EMC uses a novel coronavirus receptor for entry, can be activated  
492 by TMPRSS2, and is targeted by neutralizing antibodies. *J Virol* **87**:5502-5511.
- 493 17. **Laporte M, Naesens L.** 2017. Airway proteases: an emerging drug target for  
494 influenza and other respiratory virus infections. *Curr Opin Virol* **24**:16-24.
- 495 18. **Hatesuer B, Bertram S, Mehnert N, Bahgat MM, Nelson PS, Pohlmann S,**  
496 **Schughart K.** 2013. Tmprss2 is essential for influenza H1N1 virus pathogenesis in  
497 mice. *PLoS Pathog* **9**:e1003774.
- 498 19. **Tarnow C, Engels G, Arendt A, Schwalm F, Sediri H, Preuss A, Nelson PS,**  
499 **Garten W, Klenk HD, Gabriel G, Bottcher-Friebertshauser E.** 2014. TMPRSS2  
500 is a host factor that is essential for pneumotropism and pathogenicity of H7N9  
501 influenza A virus in mice. *J Virol* **88**:4744-4751.
- 502 20. **Sakai K, Ami Y, Tahara M, Kubota T, Anraku M, Abe M, Nakajima N,**  
503 **Sekizuka T, Shirato K, Suzaki Y, Ainai A, Nakatsu Y, Kanou K, Nakamura K,**  
504 **Suzuki T, Komase K, Nobusawa E, Maenaka K, Kuroda M, Hasegawa H,**  
505 **Kawaoka Y, Tashiro M, Takeda M.** 2014. The host protease TMPRSS2 plays a  
506 major role in in vivo replication of emerging H7N9 and seasonal influenza viruses. *J*  
507 *Virol* **88**:5608-5616.
- 508 21. **Sakai K, Sekizuka T, Ami Y, Nakajima N, Kitazawa M, Sato Y, Nakajima K,**  
509 **Anraku M, Kubota T, Komase K, Takehara K, Hasegawa H, Odagiri T,**  
510 **Tashiro M, Kuroda M, Takeda M.** 2015. A mutant H3N2 influenza virus uses an  
511 alternative activation mechanism in TMPRSS2 knockout mice by loss of an  
512 oligosaccharide in the hemagglutinin stalk region. *J Virol* **89**:5154-5158.
- 513 22. **Cheng Z, Zhou J, To KK, Chu H, Li C, Wang D, Yang D, Zheng S, Hao K,**  
514 **Bosse Y, Obeidat M, Brandsma CA, Song YQ, Chen Y, Zheng BJ, Li L, Yuen**  
515 **KY.** 2015. Identification of TMPRSS2 as a Susceptibility Gene for Severe 2009  
516 Pandemic A(H1N1) Influenza and A(H7N9) Influenza. *J Infect Dis* **212**:1214-1221.
- 517 23. **Nagata N, Iwata N, Hasegawa H, Fukushi S, Harashima A, Sato Y, Saijo M,**  
518 **Taguchi F, Morikawa S, Sata T.** 2008. Mouse-passaged severe acute respiratory

- 519 syndrome-associated coronavirus leads to lethal pulmonary edema and diffuse  
520 alveolar damage in adult but not young mice. *Am J Pathol* **172**:1625-1637.
- 521 24. **Iwata-Yoshikawa N, Uda A, Suzuki T, Tsunetsugu-Yokota Y, Sato Y, Morikawa**  
522 **S, Tashiro M, Sata T, Hasegawa H, Nagata N.** 2014. Effects of Toll-like receptor  
523 stimulation on eosinophilic infiltration in lungs of BALB/c mice immunized with  
524 UV-inactivated severe acute respiratory syndrome-related coronavirus vaccine. *J*  
525 *Viro* **88**:8597-8614.
- 526 25. **Ichinohe T, Watanabe I, Ito S, Fujii H, Moriyama M, Tamura S, Takahashi H,**  
527 **Sawa H, Chiba J, Kurata T, Sata T, Hasegawa H.** 2005. Synthetic  
528 double-stranded RNA poly(I:C) combined with mucosal vaccine protects against  
529 influenza virus infection. *J Virol* **79**:2910-2919.
- 530 26. **Trumpfheller C, Caskey M, Nchinda G, Longhi MP, Mizenina O, Huang Y,**  
531 **Schlesinger SJ, Colonna M, Steinman RM.** 2008. The microbial mimic poly IC  
532 induces durable and protective CD4+ T cell immunity together with a dendritic cell  
533 targeted vaccine. *Proc Natl Acad Sci U S A* **105**:2574-2579.
- 534 27. **Schulz O, Diebold SS, Chen M, Naslund TI, Nolte MA, Alexopoulou L, Azuma**  
535 **YT, Flavell RA, Liljestrom P, Reis e Sousa C.** 2005. Toll-like receptor 3 promotes  
536 cross-priming to virus-infected cells. *Nature* **433**:887-892.
- 537 28. **Gitlin L, Barchet W, Gilfillan S, Cella M, Beutler B, Flavell RA, Diamond MS,**  
538 **Colonna M.** 2006. Essential role of mda-5 in type I IFN responses to  
539 polyriboinosinic:polyribocytidylic acid and encephalomyocarditis picornavirus.  
540 *Proc Natl Acad Sci U S A* **103**:8459-8464.
- 541 29. **Bugge TH, Antalis TM, Wu Q.** 2009. Type II transmembrane serine proteases. *J*  
542 *Biol Chem* **284**:23177-23181.
- 543 30. **Vaarala MH, Porvari KS, Kellokumpu S, Kyllonen AP, Vihko PT.** 2001.  
544 Expression of transmembrane serine protease TMPRSS2 in mouse and human  
545 tissues. *J Pathol* **193**:134-140.
- 546 31. **Kim TS, Heinlein C, Hackman RC, Nelson PS.** 2006. Phenotypic analysis of  
547 mice lacking the Tmprss2-encoded protease. *Mol Cell Biol* **26**:965-975.
- 548 32. **Donaldson SH, Hirsh A, Li DC, Holloway G, Chao J, Boucher RC, Gabriel SE.**

- 549 2002. Regulation of the epithelial sodium channel by serine proteases in human  
550 airways. *J Biol Chem* **277**:8338-8345.
- 551 33. **Kido H, Okumura Y, Takahashi E, Pan HY, Wang S, Chida J, Le TQ, Yano M.**  
552 2008. Host envelope glycoprotein processing proteases are indispensable for entry  
553 into human cells by seasonal and highly pathogenic avian influenza viruses. *J Mol*  
554 *Genet Med* **3**:167-175.
- 555 34. **Yamaya M, Shimotai Y, Hatachi Y, Lusamba Kalonji N, Tando Y, Kitajima Y,**  
556 **Matsuo K, Kubo H, Nagatomi R, Hongo S, Homma M, Nishimura H.** 2015. The  
557 serine protease inhibitor camostat inhibits influenza virus replication and cytokine  
558 production in primary cultures of human tracheal epithelial cells. *Pulm Pharmacol*  
559 *Ther* **33**:66-74.
- 560 35. **Bertram S, Heurich A, Lavender H, Gierer S, Danisch S, Perin P, Lucas JM,**  
561 **Nelson PS, Pohlmann S, Soilleux EJ.** 2012. Influenza and SARS-coronavirus  
562 activating proteases TMPRSS2 and HAT are expressed at multiple sites in human  
563 respiratory and gastrointestinal tracts. *PLoS One* **7**:e35876.
- 564 36. **Glowacka I, Bertram S, Muller MA, Allen P, Soilleux E, Pfefferle S, Steffen I,**  
565 **Tsegaye TS, He Y, Gnirss K, Niemeyer D, Schneider H, Drosten C, Pohlmann S.**  
566 2011. Evidence that TMPRSS2 activates the severe acute respiratory syndrome  
567 coronavirus spike protein for membrane fusion and reduces viral control by the  
568 humoral immune response. *J Virol* **85**:4122-4134.
- 569 37. **Heurich A, Hofmann-Winkler H, Gierer S, Liepold T, Jahn O, Pohlmann S.**  
570 2014. TMPRSS2 and ADAM17 cleave ACE2 differentially and only proteolysis by  
571 TMPRSS2 augments entry driven by the severe acute respiratory syndrome  
572 coronavirus spike protein. *J Virol* **88**:1293-1307.
- 573 38. **Shirato K, Kawase M, Matsuyama S.** 2017. Wild-type human coronaviruses  
574 prefer cell-surface TMPRSS2 to endosomal cathepsins for cell entry. *Virology*  
575 doi:10.1016/j.virol.2017.11.012.
- 576 39. **Shulla A, Heald-Sargent T, Subramanya G, Zhao J, Perlman S, Gallagher T.**  
577 2011. A transmembrane serine protease is linked to the severe acute respiratory  
578 syndrome coronavirus receptor and activates virus entry. *J Virol* **85**:873-882.

- 579 40. **Bertram S, Glowacka I, Muller MA, Lavender H, Gnirss K, Nehlmeier I,**  
580 **Niemeyer D, He Y, Simmons G, Drosten C, Soilleux EJ, Jahn O, Steffen I,**  
581 **Pohlmann S.** 2011. Cleavage and activation of the severe acute respiratory  
582 syndrome coronavirus spike protein by human airway trypsin-like protease. *J Virol*  
583 **85**:13363-13372.
- 584 41. **Simmons G, Zmora P, Gierer S, Heurich A, Pohlmann S.** 2013. Proteolytic  
585 activation of the SARS-coronavirus spike protein: cutting enzymes at the cutting  
586 edge of antiviral research. *Antiviral Res* **100**:605-614.
- 587 42. **Zhou Y, Vedantham P, Lu K, Agudelo J, Carrion R, Jr., Nunneley JW, Barnard**  
588 **D, Pohlmann S, McKerrow JH, Renslo AR, Simmons G.** 2015. Protease  
589 inhibitors targeting coronavirus and filovirus entry. *Antiviral Res* **116**:76-84.
- 590 43. **Blasius AL, Beutler B.** 2010. Intracellular toll-like receptors. *Immunity*  
591 **32**:305-315.
- 592 44. **Lappi-Blanco E, Soini Y, Kinnula V, Paakko P.** 2002. VEGF and bFGF are highly  
593 expressed in intraluminal fibromyxoid lesions in bronchiolitis obliterans organizing  
594 pneumonia. *J Pathol* **196**:220-227.
- 595 45. **van den Brand JM, Smits SL, Haagmans BL.** 2015. Pathogenesis of Middle East  
596 respiratory syndrome coronavirus. *J Pathol* **235**:175-184.
- 597 46. **Ng DL, Al Hosani F, Keating MK, Gerber SI, Jones TL, Metcalfe MG, Tong S,**  
598 **Tao Y, Alami NN, Haynes LM, Mutei MA, Abdel-Wareth L, Uyeki TM,**  
599 **Swerdlow DL, Barakat M, Zaki SR.** 2016. Clinicopathologic,  
600 Immunohistochemical, and Ultrastructural Findings of a Fatal Case of Middle East  
601 Respiratory Syndrome Coronavirus Infection in the United Arab Emirates, April  
602 2014. *Am J Pathol* **186**:652-658.
- 603 47. **Markan KR, Potthoff MJ.** 2016. Metabolic fibroblast growth factors (FGFs):  
604 Mediators of energy homeostasis. *Semin Cell Dev Biol* **53**:85-93.
- 605 48. **Kuhn N, Bergmann S, Kosterke N, Lambertz RLO, Keppner A, van den Brand**  
606 **JMA, Pohlmann S, Weiss S, Hummler E, Hatesuer B, Schughart K.** 2016. The  
607 Proteolytic Activation of (H3N2) Influenza A Virus Hemagglutinin Is Facilitated by  
608 Different Type II Transmembrane Serine Proteases. *J Virol* **90**:4298-4307.

- 609 49. **Simeoni L, Rufini A, Moretti T, Forte P, Aiuti A, Fantoni A.** 2002. Human CD26  
610 expression in transgenic mice affects murine T-cell populations and modifies their  
611 subset distribution. *Hum Immunol* **63**:719-730.

612

613

614 **Figure legends**

615 **FIG 1.** Genotyping of C57BL/6 (WT), TMPRSS2-KO (KO), hDPP4-Tg (Tg) and  
616 TMPRSS2-KO hDPP4 (KO-Tg) mice by PCR analysis. PCR analysis was performed on  
617 the genomic DNA from ear punches taken from WT, KO, Tg, and KO-Tg mice (WT,  
618 4-5-week-old, n=3, [male=3]; KO, 4-5-week-old, n=3, [male=3]; Tg, 4-5-week-old, n=3,  
619 [male=1, female=2]; KO-Tg, 4-5-week-old, n=3, [male=1, female=2]), and the resulting  
620 products (391 bp for hDPP4 and 388 bp for TMPRSS2) are shown. Numbers indicate  
621 positions of the 500 bp standard molecular weight marker ladder. M, 100 bp ladder; P,  
622 positive controls for hDPP4 or TMPRSS2; N, negative control without the ear punch  
623 template.

624

625 **FIG 2.** Experimental infection of TMPRSS2-knockout (KO) mice with SARS-CoV.

626 C57BL/6 (WT) and TMPRSS2-KO mice were inoculated with F-musX (SARS-CoV). (a)  
627 Body weight curve during the first 10 days post-infection (p.i.). Numbers of animals per  
628 group were as follows: KO, n=14 (male=11, female=3); WT, n=10 (male=5, female=5).

629 Mice of 22-28 weeks-old were used. Error bars represent standard errors. \*,  $p < 0.05$ ; \*\*\*\*,  
630  $p < 0.0001$  (one-way ANOVA.). (b) Virus titer in lungs from SARS-CoV-inoculated animals  
631 at 6 h and at 1, 2, and 3 days p.i. Numbers of animals per group were as follows: KO,  $n = 4-5$   
632 per time point (male=0-1, female=3-4); WT,  $n = 4-5$  per time point (male=0-1, female=3-4).  
633 Mice of 14-30 weeks-old were used. Error bars represent standard errors. The dotted line  
634 indicates the limit of detection. P-values in the graph were calculated by two-way ANOVA  
635 to determine significant effects of viral titers in different animal strains at different time  
636 points. (c) Neutralizing antibody titer in serum on Day 10 p.i. The data are from the same  
637 animals used in (a), except for one mouse that died. Each symbol represents an individual  
638 mouse. Numbers of animals per group were as follows: KO,  $n = 14$  (male=11, female=3);  
639 WT,  $n = 9$  (male=4, female=5). Mice of 22-28 weeks-old were used. Error bars represent  
640 standard errors. P-values for the graph were calculated by the Mann-Whitney test. The  
641 dotted line indicates the limit of detection. (d) Histopathological examination of the lungs  
642 from WT and TMPRSS2-KO mice after infection by SARS-CoV. Numbers of animals per  
643 group were as follows: KO,  $n = 3$  per time point (male=1-2, female=1-2); WT,  $n = 3$  per time

644 point (male=1-2, female=1-2). Mice of 15-20 weeks-old were used. Representative images  
645 of lungs from mice on Days 1 and 3 days p.i. Immunohistochemical analysis using an  
646 anti-SARS-CoV polyclonal antibody (at 1 and 3 days p.i.). Hematoxylin and eosin staining  
647 at 3 days p.i. On Day 1 p.i., viral antigen-positive cells are seen mainly in the bronchi of a  
648 WT mouse, whereas very weakly positive cells are seen in a TMPRSS2-KO mouse (left  
649 panels, brown color). On Day 3 p.i., several alveolar cells around the bronchi in both WT  
650 and TMPRSS2-KO mice are positive for viral antigen (middle panels, brown color). Cell  
651 debris and diffuse inflammatory infiltration by neutrophils and mononuclear cells are seen  
652 around bronchi and in the alveolar area of WT mice, whereas focal inflammatory  
653 infiltration is observed in the alveoli of TMPRSS2-KO (right panels, inset). Br, bronchi; Al,  
654 alveolar area; V, vein. Bars, 20 or 200  $\mu$ m.

655

656 **FIG 3.** Formation of granulation tissue in TMPRSS2-knockout (KO) mice after infection  
657 with SARS-CoV. Histopathological examination of the lungs from WT and TMPRSS2-KO  
658 mice at 10 days after infection with SARS-CoV. Representative images of lungs are from

659 the same animals in Fig. 2a. HE, Hematoxylin and eosin staining; MT, Masson's trichrome  
660 staining. Granulation tissue, known as Masson bodies (blue allows in HE; Red arrows in  
661 MT) was located in the alveolar duct walls of WT mice, but to a lesser extent in  
662 TMPRSS2-KO mice. Br, bronchi; Ad, Alveolar duct; Al, alveolar area. Bars, 200 or 100  
663  $\mu\text{m}$ .

664

665 **FIG 4.** Immune responses in TMPRSS2-knockout (KO) mice after infection with  
666 SARS-CoV. C57BL/6 wild-type (WT) and TMPRSS2-KO mice were inoculated with  
667 F-musX (SARS-CoV). Cytokine and chemokine responses (a) and the levels of type I IFN  
668 and TLR3 mRNA expression (b) in the lungs at 6 h and at 1, 2, and 3 days p.i. The lung  
669 homogenates were from the same animals in Fig 1(b) and assays were done using unicate  
670 samples per animal. Expression of each gene was normalized to that of  $\beta$ -actin in (b).  
671 Numbers of animals per group were as follows: KO, n=4 per time point (male=0-1,  
672 female=3-4); WT, n=4 per time point (male=0-1, female=3-4). Mice of 14-30 weeks-old  
673 were used. Error bars represent standard errors. P-values for the graph were calculated by

674 ANOVA. \*,  $p < 0.05$ ; \*\*,  $p < 0.01$ ; \*\*\*\*,  $p < 0.0001$ .

675

676 **FIG 5.** Experimental infection of TMPRSS2-knockout hDPP4-transgenic (KO-Tg) mice

677 with MERS-CoV. hDPP4-Tg (Tg) and KO-Tg mice were inoculated with EMC-HCoV

678 (MERS-CoV). (a) Body weight curve during the 14 days post-infection (p.i.). Numbers of

679 animals per group were as follows: KO-Tg,  $n=8$  (male=2, female=6); Tg,  $n=6$  (male=3,

680 female=3). Mice of 12-14 weeks-old were used. Error bars represent standard errors. \*\*\*,

681  $p < 0.001$  (one-way ANOVA) (b) Virus titer in the lungs of MERS-CoV-inoculated animals

682 at 6 h and at 1, 2, and 3 days p.i. Numbers of animals per group were as follows: KO-Tg,

683  $n=4$  per time point (male=0-1, female=3-4); Tg,  $n=4$  per time point (male=1-2, female=2-3).

684 Mice of 13-22 weeks-old were used. Error bars represent standard errors. The dotted line

685 indicates the limit of detection. P-values indicated in the graph were calculated by two-way

686 ANOVA for significant effects of viral titers in different animal strains at different time

687 points. (c) Neutralizing antibodies in serum from mice on Day 14 p.i. The sera were from

688 the same animals in (a). Numbers of animals per group were as follows: KO-Tg,  $n=8$

689 (male=2, female=6); Tg, n=6 (male=3, female=3). Mice of 12-14 weeks-old were used.

690 Error bars represent standard errors. \*,  $p < 0.05$ . P-values in the graph were calculated by the

691 Mann-Whitney test. The dotted line indicates the limit of detection. (d) Histopathological

692 examination of the lungs of Tg mice and TMPRSS2-KO Tg mice after infection with

693 MERS-CoV. Numbers of animals per group were as follows: KO-Tg, n=3 per time point

694 (male=1-2, female=1-2); WT, n=3 per time point (male=2-3, female=0-1). 19-25 weeks-old

695 mice were used. Representative images from mice taken on Days 1, 3, and 7 p.i.

696 Immunohistochemical analysis at 1 and 3 days p.i. using an anti-MERS-CoV nucleocapsid

697 polyclonal antibody. Hematoxylin and eosin staining at Day 7 p.i. Viral antigen-positive

698 cells are seen both in the bronchi and alveoli of a Tg mouse (left panels, brown color).

699 Some pneumocytes in the Tg mouse are positive for viral antigen, but negative in a

700 TMPRSS2-KO Tg mouse (Day 1 p.i.; left panels, brown color). Several viral

701 antigen-positive cells are seen in the alveoli and bronchi of a Tg mouse on Day 3 p.i., but

702 fewer are present in a TMPRSS2-KO Tg mouse (middle panels, brown color). On Day 7,

703 massive cellular proliferation is observed in the alveoli of a Tg mouse, with numerous

704 macrophages and mononuclear cells (right panels, inset). By contrast, multinuclear cells  
705 (including neutrophils and eosinophils) are seen in the alveoli of a TMPRSS2-KO Tg  
706 mouse (right panels, inset, arrows). Br, bronchi; Al, alveolar area; V, vein. Bars, 20 or 200  
707  $\mu\text{m}$ .

708

709 **FIG 6.** Recovery from acute pneumonia without granulation tissue in TMPRSS2-knockout  
710 hDPP4-transgenic (KO-Tg) mice with MERS-CoV. Histopathological examination of the  
711 lungs from hDPP4-Tg (Tg) and KO-Tg mice 14 days after infection with MERS-CoV.  
712 Representative images of lungs are from the same animals in Fig. 5a. HE, Hematoxylin and  
713 eosin staining; MT, Masson's trichrome staining. A lymphocyte aggregate (\*) and cellular  
714 infiltrations persisted in the alveolar area of the Tg mouse, whereas infiltrations in KO-Tg  
715 mice were mild. No granulation tissues were detected in these mice. Br, bronchi; Al,  
716 alveolar area; Bars, 200 or 100  $\mu\text{m}$ .

717

718 **FIG 7.** Immune responses in TMPRSS2-knockout (KO) hDPP4-transgenic mice after

719 infection with MERS-CoV. hDPP4-Tg (Tg) and TMPRSS2-KO hDPP4 (TMPRSS2-KO  
720 Tg) mice were inoculated with EMC-HCoV (MERS-CoV). (a) The lung homogenates were  
721 from the same animals in Fig 5(b) and assays were done using unicate samples per animal.  
722 The dotted line indicates the limit of detection. (b) The levels of type I IFN and TLR3  
723 mRNA expression in the lungs at 6 h and at 1, 2, and 3 days p.i. Numbers of animals per  
724 group were as follows: KO-Tg, n=4 per time point (male=0-1, female=3-4); Tg, n=4 per  
725 time point (male=1-2, female=2-3). Mice of 13-22 weeks-old were used. Expression of  
726 each gene was normalized to that of  $\beta$ -actin. Error bars represent standard errors. P-values  
727 for the graph were calculated by ANOVA. \*,  $p<0.05$ ; \*\*,  $p<0.01$ .

728

729 **FIG 8.** Immune responses after intranasal inoculation of mice with poly (I:C).

730 Concentrations of inflammatory cytokines and chemokines in the lungs at 24 h

731 post-infection. The assays were done using unicate samples per animal. Numbers of

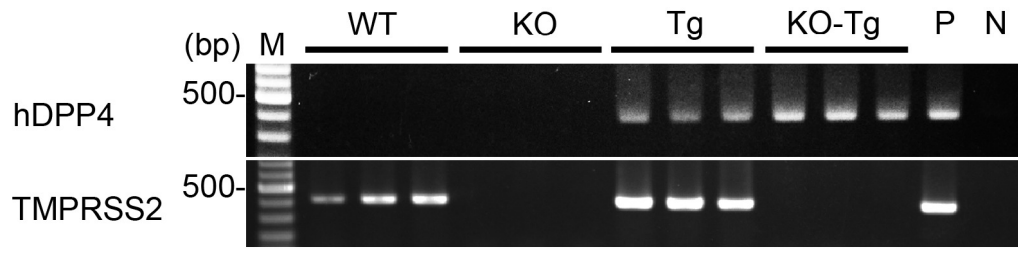
732 animals per group were as follows: WT, n=4 per group (male=2, female=2); KO, n=4 per

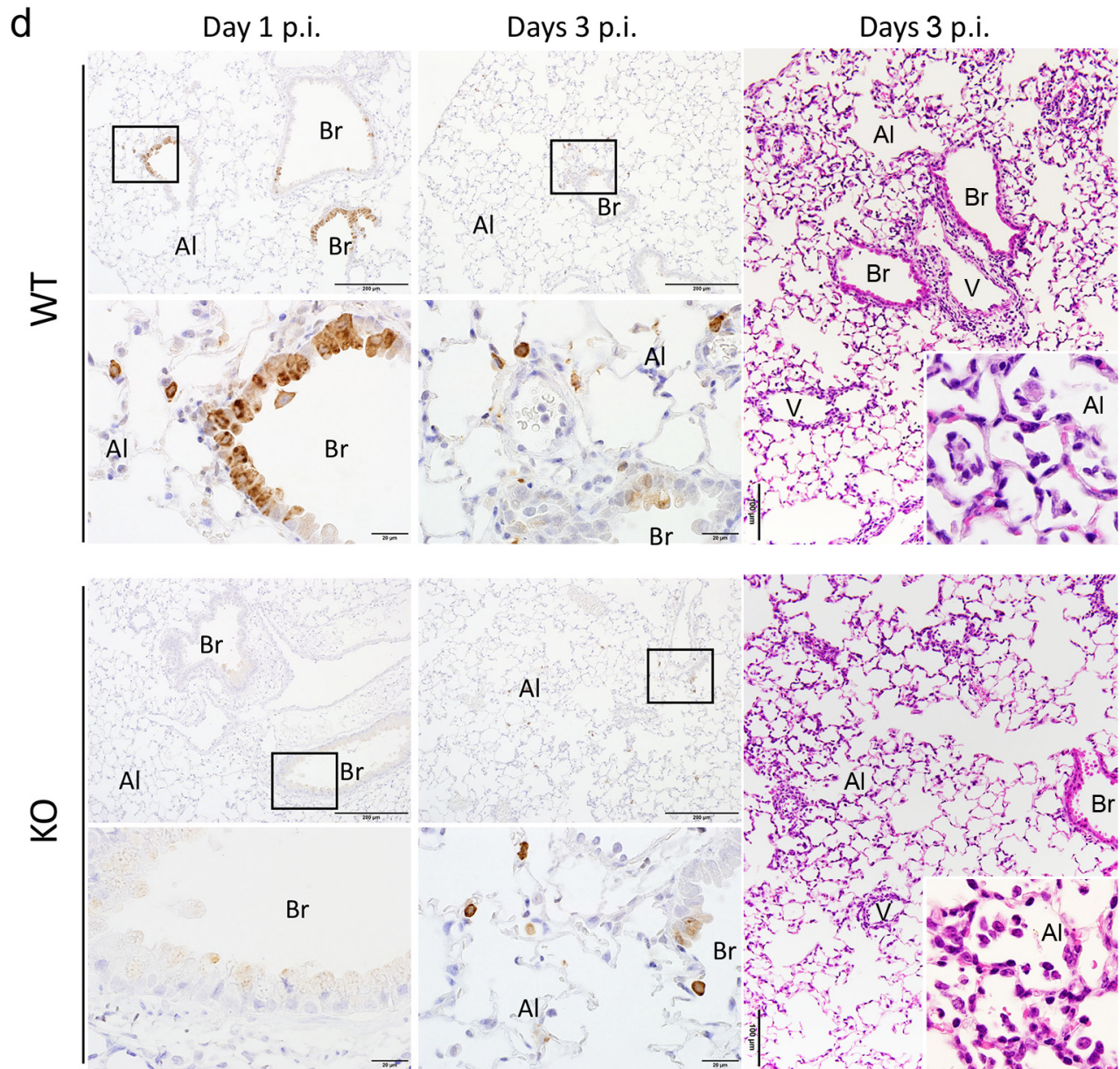
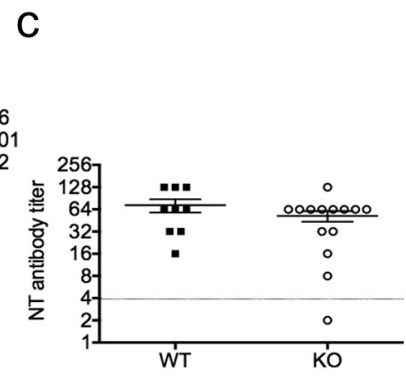
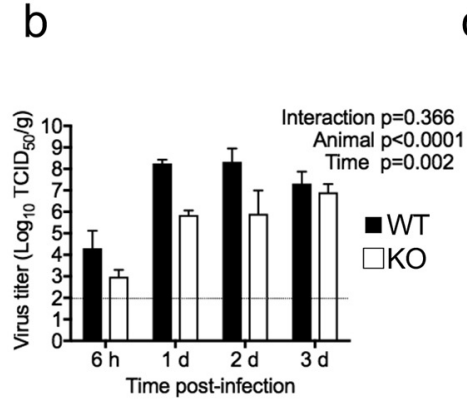
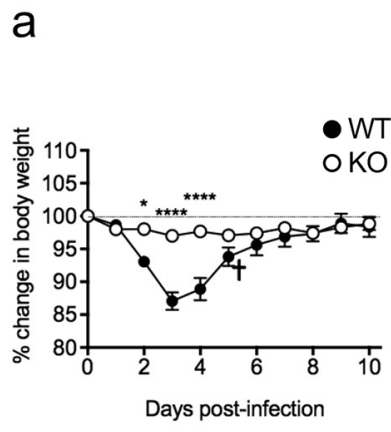
733 group (male=2, female=2); Tg, n=4 per group (male=2, female=2); KO-Tg, n=4 per group

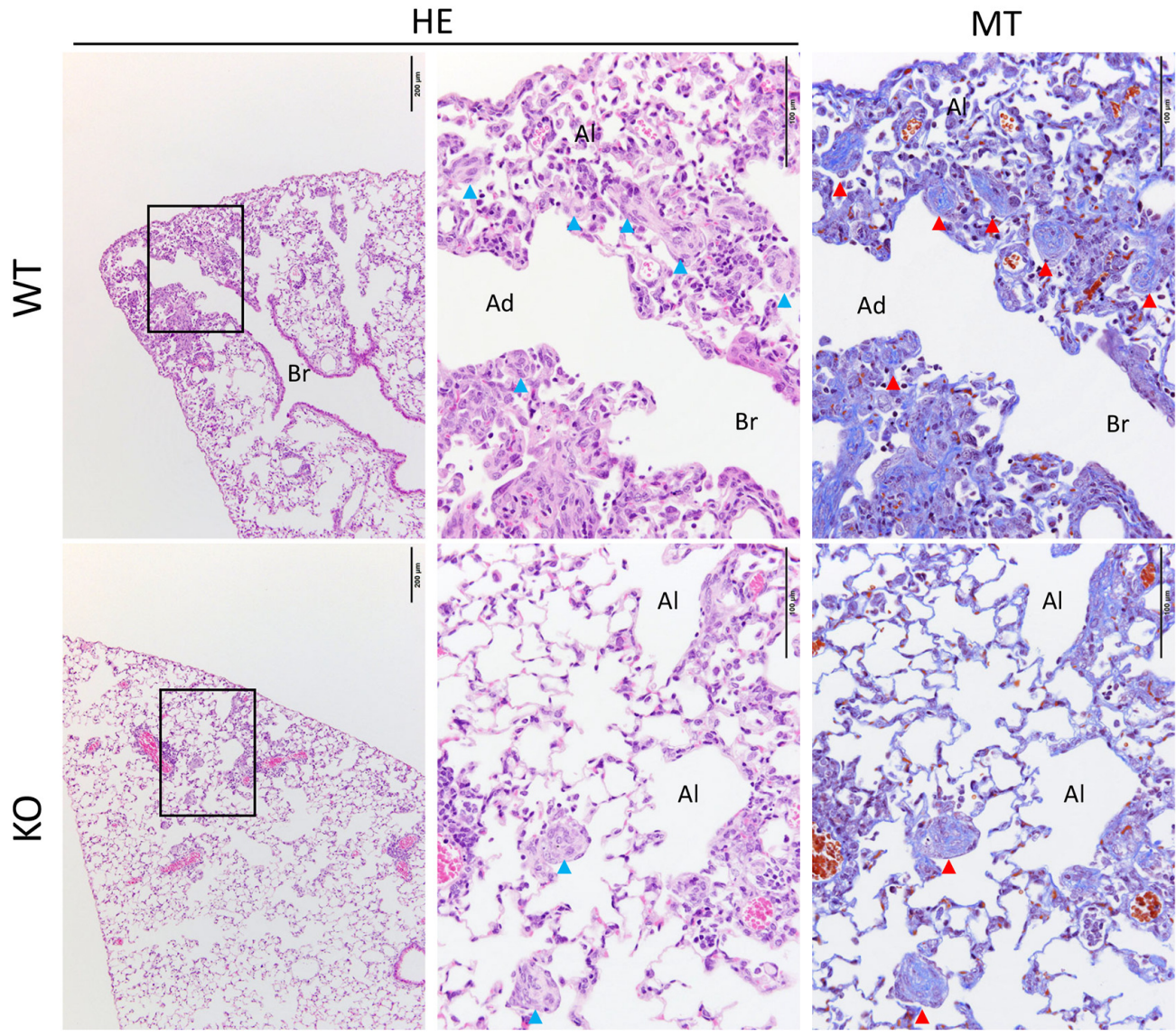
734 (poly I:C, male=2, female=2; PBS, male=1, female=3). Mice of 14-16 weeks-old were used.

735 Error bars represent standard errors. P-values for the graph were calculated by ANOVA. \*,

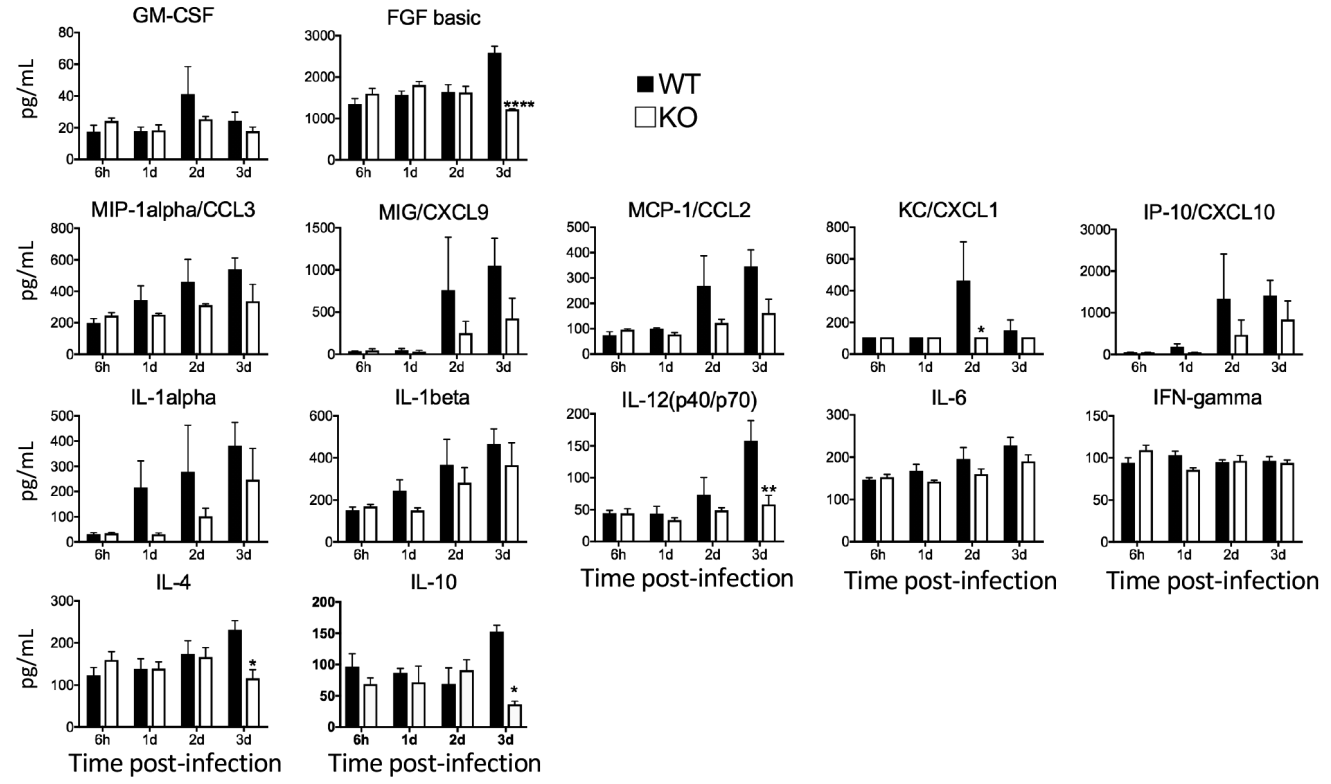
736  $p < 0.05$ .



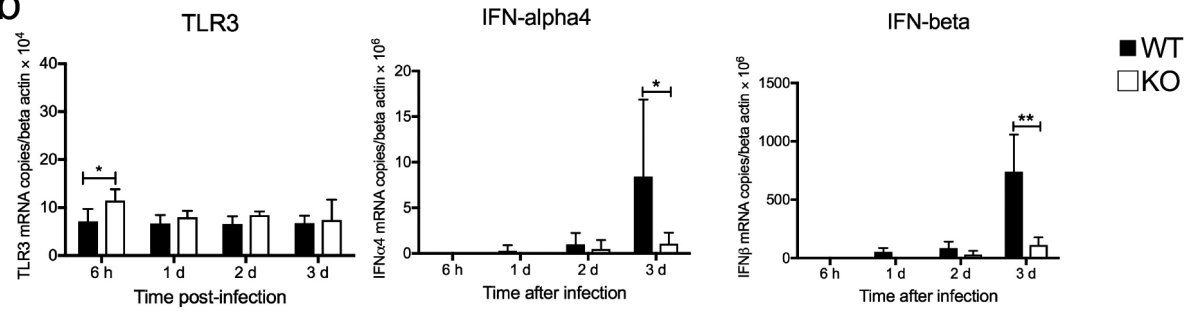




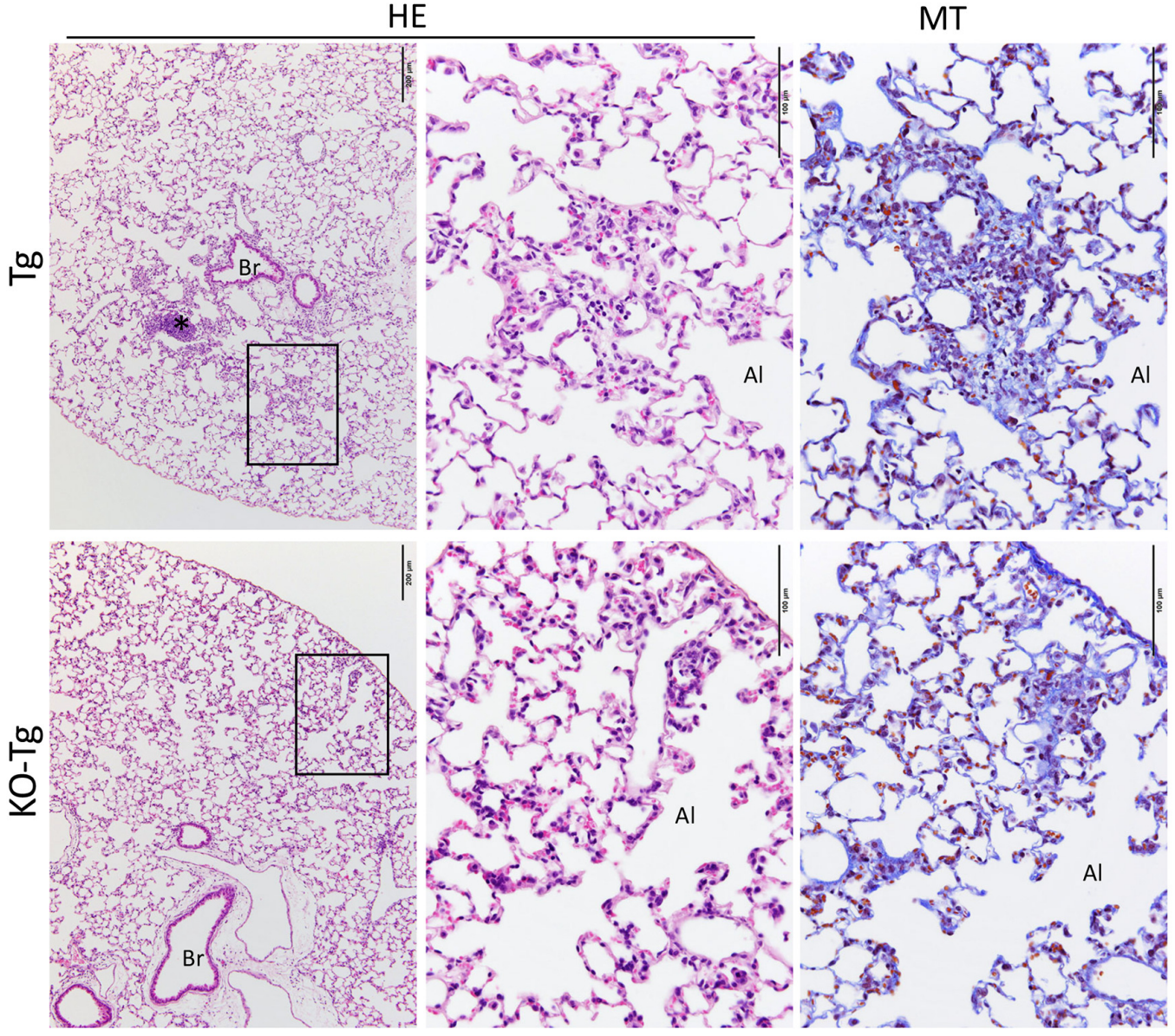
a



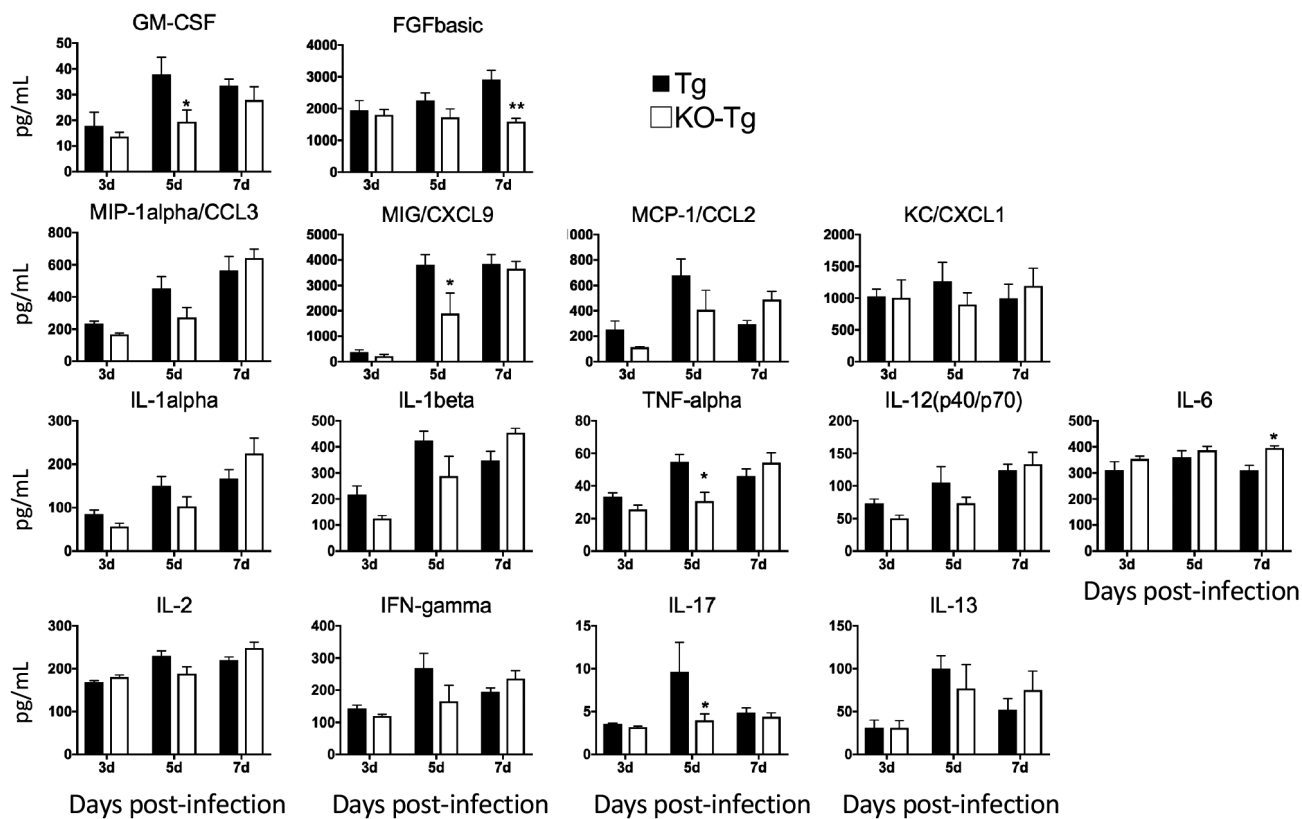
b







**a**



**b**

